Strouhal number effects on pulsating synthetic jet's entrainment

Andrea Dal Monte[1] *, Andrea Battiston[2] †, Rita Ponza[2] ‡,
Francesco De Vanna[1] §, Francesco Picano[1] ¶, Ernesto Benini[1] ‖
[1]*University of Padova, Department of Industrial Engineering, Via Venezia 1, 35131 Padova, Italy*
[2]*Hit09, Piazzetta Bettiol 15, 35123 Padova, Italy*

In the context of the active flow control of a massively separated flow through synthetic pulsed jets, the ability to determine a correspondence between the pulsation and the desired mean velocity is of prime interest and a crucial target. In the present work, an approach based on the actual mean speed and the entrained fluid in the jet is proposed using the state-of-the-art entrainment rate metrics in the evaluation. In particular, numerical simulations of a representative simplified case are performed in several conditions; the analyses are carried out using a commercial CFD solver by solving both the steady and unsteady Reynolds-Averaged Navier-Stokes system of equations closed by $k-\omega$ SST turbulence model. The study aims at determining the equivalent steady jet that provides similar entrainment effects of an unsteady setup.

I. Nomenclature

CFD	=	Computational Fluid Dynamics
$DPIV$	=	Digital Particle Image Velocimetry
DNS	=	Direct Numerical Simulation
LCS	=	Lagrangian Coherent Structure
$MUSCL$	=	Monotonic Upstream-centered Scheme for Conservation Laws
$PLIF$	=	Planar Laser-Induced Fluorescence
PIV	=	Particle Image Velocimetry
SJ	=	Synthetic Jet
SST	=	Shear Stress Transport
$URANS$	=	Unsteady Reynolds Averaged Navier-Stokes
$ZNMF$	=	Zero Net Mass Flux

II. Introduction

NOWDAYS, aerodynamic optimisation of civil aircraft is an increasingly and demanding task for aeronautical applications. It is well known that a more in-depth comprehension of near-wall fluid mechanics has led to many applicative lapels in the field of controlling and stabilising the boundary layer, thus accounting for better prototyping the near-future flight vehicles. Among the various technologies which aim at reducing the flying drag and broad the operative ranges, the adoption of Synthetic Jets (SJs) with Zero-Net Mass-Flux (ZNMF) is one of the most promising technologies. In particular, this technique allows enhancing the suction side wing performance under high angle of attack and low speed, granting significant improvements of the aerodynamic system performance during take-off, initial climbing and landing flight phases.

The SJ approach falls in the field of fluid entrainment during vortex ring formation, a topic that has seen several contributions and increasingly advanced studies in the last decades. In this context, Han and Mungal [1] directly measured the entrainment of a turbulent jet in co-flow using Particle Image Velocimetry (PIV). The study focused on

*Post-Doc, Department of Industrial Engineering, andrea.dalmonte@unipd.it
†R&D engineer, Hit09 Srl, a.battiston@hit09.com
‡CEO, Hit09 Srl, r.ponza@hit09.com
§Lecturer, Department of Industrial Engineering, francesco.devanna@unipd.it
¶Professor, Department of Industrial Engineering, francesco.picano@unipd.it
‖Professor, Department of Industrial Engineering, ernesto.benini@unipd.it, Member AIAA

the investigation of the effects of different parameters on jet's entrainment. In addition, the authors described how the jet entrainment is reduced by the co-flow speed as well as the heat release was found to cut down the entrainment by a 2.5 factor while buoyancy recovers the entrainment to a faster rate. Dabiri and Gharib [2] measured the entrainment in an isolated vortex ring using a coaxial counterflow with the aim of delaying the translation of the vortex generated from a piston-cylinder mechanism. The unsteady vortex ring boundaries were identified with the instantaneous streamlines, and such a technique was also used to compute the fluid entrainment. Olcay and Krueger [3] used Planar Laser-Induced Fluorescence (PLIF) and Digital Particle Image Velocimetry (DPIV) combined with Lagrangian Coherent Structure (LCS) techniques to measure ambient entrainment during laminar vortex ring formation. The observed trends in entrainment and final entrained fluid fraction are explained and presented. Raju et al. [4] proposed a model based on only the slot of ZNMF jets in grazing flows for flow control simulations. The characteristics of the jet are expressed in terms of mean integral quantities; the model is compared with a full cavity simulation and with the sinusoidal, plug-flow model. The results show a correct prediction of the jet effect on the separation bubble. El Hassan and Meslem [5] adopted the stereoscopic particle image velocimetry technique to estimate the entrainment in the near field of circular and daisy-shaped orifice jets. The analyses highlight a strong correlation between the entrainment and the Kelvin–Helmholtz vortex dynamics for the circular jet at a fixed Reynolds number. Finally, the flow dynamics and, in particular, the vortex behaviour are described. Sau and Mahesh [6] used Direct Numeric Simulations (DNS) to describe the mixing behaviour of pulsed jets in crossflow. Different velocity ratios are considered, and an optimal curve in the space of stroke and velocity ratios is calculated. Möller et al. [7] used a de-aeration system to conduct quasi-continuous measurements of the amount of entrained air due to intake vortices. The experimental analysis allowed to identify the mean air entrainment at horizontal intakes, and empirical equations were proposed with regression tools. Berk et al. [8] investigated the effect of different frequencies, hence of the Strouhal number, on periodic forcing of the flow over a backwards-facing step. The variations of the entrainment are related to the Strouhal number, and a technique based on the analysis of the unsteady flow field is presented to estimate the mean entrainment value during a jet phase. Finally, Stella et al. [9] proposed a model for separated flows based on mass entrainment; the model of the mean flow consists of a stationary vortex scaled with the mean recirculation length. The mean mass entrainment is calculated and used to predict the mean properties of separated flows.

In this context, the X-Pulse program in the Clean Sky 2 Joint Undertaking [10] aims at developing a novel model for pulsating SJ, providing a suitable steady-state reduced model with equivalent entrainment level of a realistic unsteady jet. Thus, in the present investigation, the results of the unsteady analyses of the crossflow jet, at different frequencies, are post-processed using a variation of the technique proposed by Berk et al. [8]. The results are compared in terms of mean entrainment during a phase with a steady-state analysis to match the velocity values that produce a similar entrainment value. The work aims at marking (*i*) the most significant difference between the effect of a steady jet and a pulsed jet on re-energising the boundary layer and (*ii*) investigating the additional outer-to-jet fluid entrainment resulting from the starting jet, and more particularly from the *mushroom-shaped* head of the starting jet. In particular, once the starting jet is sufficiently developed, its influence on the outer-to-jet fluid entrainment strongly diminishes due to the saturation of the vorticity level contained in the toroidal vortex constituting the head of the jet. Downstream, the pulsed jet exhibits similar-to-steady-jet characteristics. In this concerns, a steady pulse jet model is developed in such a way as to consider the additional entrainment through a corresponding increase in the blowing velocity. In particular, the blowing velocity of the steady jet is defined such that the momentum surplus injected in the boundary layer on a time-lap equals a whole period of blowing/suction of the pulsed jet. The entrainment effects results to be the same as the momentum surplus injected during the blowing phase for the pulsed jets and all the sources of entrainment of outer-to-jet fluid are also taken into account. The main difference between the steady and the pulsed jet is a starting jet instability that promotes additional entrainment for a limited time.

The present work is organised as follow: Section III describes the geometry and the numerical model employed in the analysis. Section IV details the results obtained with the non-stationary jet as a function of the Strouhal number. Section V describes the equivalent jet steady-state model, which allows for equivalent momentum injection in the flow domain. Finally, Section VI states the conclusive remarks.

III. Numerical model and Solution strategy

The present study is carried using Ansys Fluent. In particular, the geometrical characteristics of the numerical model is represented by the sketch in Figure 1. The model consists of two main parts: the flow domain and the actuator body, where the jet boundary conditions are enforced.

The flow domain extents for $L_x \times L_y \times L_z = (85 \times 8 \times 12) r_x$, being r_x the actuator radius along with the streamwise

coordinate. The flow domain is discretised with a zone of non-uniform Cartesian mesh stretched in correspondence to the lower wall and a polyhedral mesh in the upper part. The overall number of elements is 6 million. Concerning the actuator's dimensions, the latter elliptically shaped, sizes $(1 \times 0.2)r_x$, with $r_x = 0.0125\ m$.

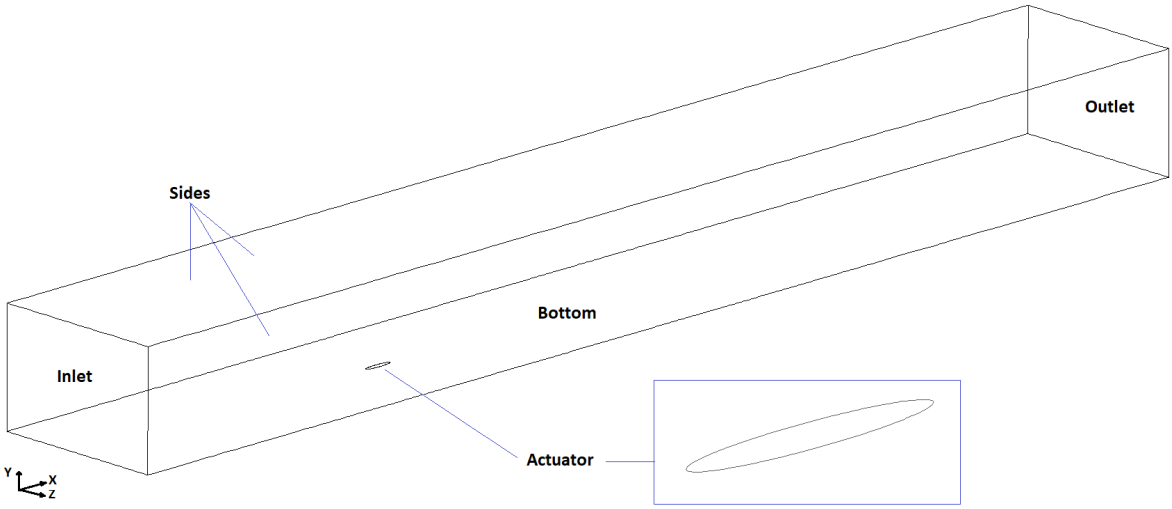

Fig. 1 Geometrical representation of the computational domain.

The system dynamics is analysed by solving the Unsteady Reynolds Averaged Navier-Stokes (URANS) system of equations. Turbulence modelling is demanded to a standard $k - \omega$ SST closure. A 3rd order MUSCL scheme is used to treat the spatial components of the Navier-Stokes equations, while the Fluent standard implementation of the Least Squares Cell-Based approach is used for gradients' reconstruction. Temporal integration is made by a first-order implicit scheme, setting the inner iteration number to 20. As far as the steady-state simulations, which are subsequently performed in light of finding the equivalent steady configuration of the unsteady set, the latter are run till the convergence of the whole set of evolutionary variables. The convergence is measured by setting a precomputed tolerance of 1E-5, the latter used as a stop mark for the iterative Navier-Stokes residuals dropping. The process takes about 1500 iterations per steady-state analysis.

As far as the flow domain, the boundary conditions are specified as follow: at the inlet location, the mass flow rate is enforced through a *mass flow inlet condition* and setting the reference Mach number M_∞ equal to 0.23. At the outlet location, a pressure-outlet condition is adopted prescribing a static pressure of $p_{out} = 101325\ Pa$. The bottom surface, corresponding to the wing piece where the SJ is supposed to be installed, is treated as a non-slip and adiabatic wall. Symmetry conditions are enforced along with the rest of the domain sides. The choice is found to be not particularly invasive since the position of the lateral and upper boundary conditions is placed sufficiently far from the actuator location, making the symmetry condition non-intrusive concerning the fluid phenomena under observation. The boundary conditions, as well as the solver set up, are summarised in Table 1.

The actuator is modelled with both mass flow-inlet and outlet, depending on its role concerning the main flow. As far as the unsteady configuration is concerned, the analysis is performed by varying the actuating inflow condition with a sinusoidal monochromatic law, ensuring the inflowing speed to be equal to

$$V(t) = V_0 \sin(\omega t) \tag{1}$$

Here $V_0 = 403.2\ m/s$ is the SJ reference outflowing speed, $\omega = 2\pi f$ is the jet's angular frequency, where f denotes wave frequency. The analysis focuses on the SJ entrainment effect by varying the Strouhal number, i.e. $St = f r_x / V_\infty$, so that the jet's frequency is varied in the range from 1500 Hz up to 2600 Hz, being $V_\infty = 78.24\ m/s$ the free stream outer velocity.

An overall view concerning the flow organisation in a time-dependent case is reported in Figure 2. Here, in particular, the Q-criterion for vorteces visualisation shows the 10 iso-countors of the second invariant of velocity gradient applied to the $St = 0.28$ pulsating jet.

Fluid Domain			
Inlet	Mass flow inlet (M = 0.23)	**Outlet**	Static pressure (p_{out} = 101325 Pa)
Bottom	No slip wall	**Sides**	Symmetry
Actuator Conditions			
Actuator	Mass flow-inlet / Mass flow-outlet V_0 = 403.2 m/s f = 1500 ÷ 2600 Hz		
Discretization Schemes			
Gradient	Least Squares Cell Based	**Flow**	3rd Order MUSCL
k	3rd Order MUSCL	**Omega**	3rd Order MUSCL
Time	1st order Implicit		

Table 1 Boundary Conditions and Discretization Schemes

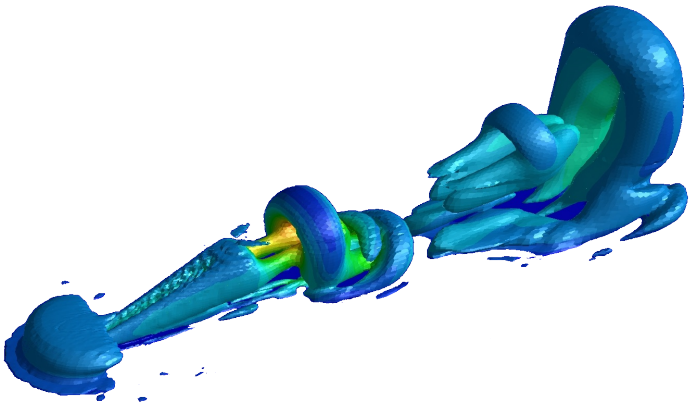

Fig. 2 Q-criterion contour plots at $\Phi = 150°$ of the $St = 0.28$ pulsating jet.

The proposed numerical method is validated from the experimental study of SJA/cross-flow interaction provided by CFDVAL2004 [11]. The workshop provides the actuator geometries, the structured-hex and unstructured-tetra meshes, inlet conditions and membrane motion from experimental data. Furthermore, the time-averaged experimental data are provided at various locations. Three different strategies are tested in the previous activities of X-Pulse Project [10] to simulate, in a steady approach, i) the whole actuator, ii) the actuator as a surface boundary condition and iii) the actuator as a volumic body force. The results in terms of *normal to plane velocity* profiles at different streamwise locations and vortices positions are compared and a good agreement between the different approaches is found.

IV. Results of unsteady cross-flow case

The section presents the results of the unsteady pulsating jets analyses. Four frequencies are mined in order to characterise the system dynamics; thus, the corresponding Strouhal number in the set $St = \{0.23, 0.28, 0.31, 0.41\}^T$ is used for the subsequent cases' description.

Before proceeding in reporting the results, a brief description of the entrainment calculation criterion is here presented. The latter follows the method proposed by Berk et al. [8]. In particular, since the alternating train of

vortices and the corresponding alternating jet-normal velocity component lead to momentum entrainment into the recirculation region, the flow motion orthogonal to the main jet direction, from external field to jet centreline, injects high-momentum fluid in the recirculation region. In contrast, the motion from the jet centreline to the external field removes low-momentum fluid from the recirculation region. Thus, to determine the entrainment, the $x - y$ plane, containing the streamwise actuator axis, is considered, and the velocity components orthogonal to a reference line, pointing towards the jet centreline, are conditionally averaged across all the jet phases. In the present analysis, the reference line starts from a distance of the 5% of streamwise actuator length upwind the actuator border and inclines $\alpha = 20°$. Such a setup, according to Berk et al. [8], allows computing the entrainment velocity as:

$$V_{en} = -\frac{V_{line}}{V_{\infty} sin(\alpha)} - 1 \tag{2}$$

being, V_{line} the fluid speed along with the precomputed α-inclined line

$$V_{line} = V_y cos(\alpha) - V_x sin(\alpha) \tag{3}$$

The computations results are reported in the following. In particular, the authors express them as a function of the streamwise coordinate, parametrically with the Strouhal number. Figs. 3, 4, 5 and 6 show the evolution of V_{en} along with the reference line, during a whole period. For the sake of clarity, the complete period is divided into blowing ($\Phi = 0 \div 180°$) and suction ($\Phi = 180 - 360°$) phases.

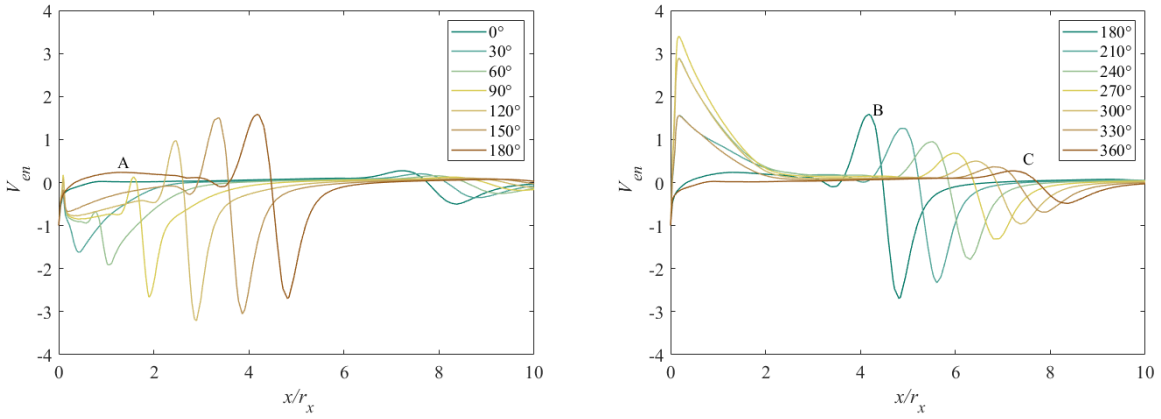

(a) Blowing phase: $\phi = 0 \div 180°$ (b) Suction phase: $\phi = 180 \div 360°$

Fig. 3 St = 0.23, evolution of V_{en} during one period

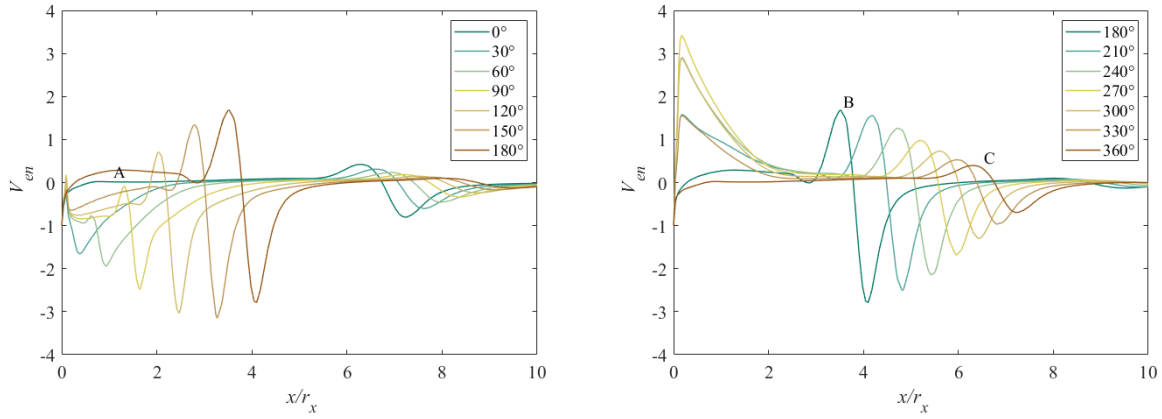

(a) Blowing phase: $\phi = 0 \div 180°$ (b) Suction phase: $\phi = 180 \div 360°$

Fig. 4 St = 0.28, evolution of V_{en} during one period

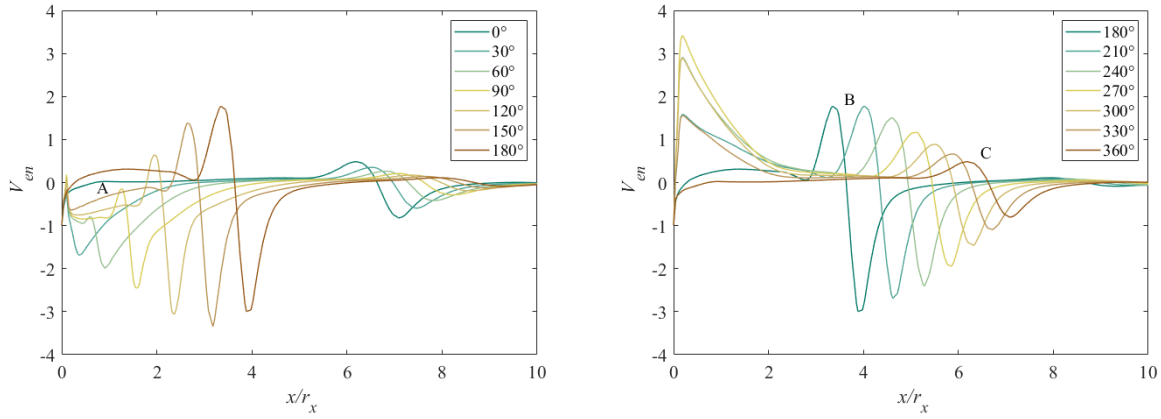

(a) Blowing phase: $\phi = 0 \div 180°$ (b) Suction phase: $\phi = 180 \div 360°$

Fig. 5 St = 0.31, evolution of V_{en} during one period

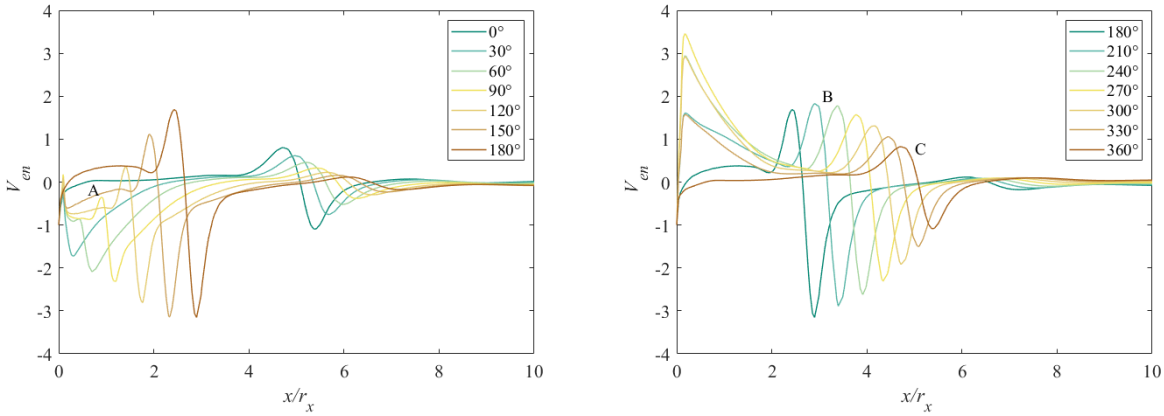

(a) Blowing phase: $\phi = 0 \div 180°$ (b) Suction phase: $\phi = 180 \div 360°$

Fig. 6 St = 0.41, evolution of V_{en} during one period

The analysis of entrainment value along with the reference line reveals two peaks of V_{en} during the jet period: the first evolves with the jet's front, the second is located in the proximity of the origin line. The first peak moves downwind as the jet evolves in time; however, some differences are observed increasing the jet frequency. At first, the positive peak of V_{en} makes its appearance at $\Phi = 90°$ for $St = 0.23$ while it is delayed, in phase, when the frequency increases ($\Phi = 105°$ for $St = 0.31$ and $\Phi = 120°$ for $St = 0.41$) and the streamwise location remains unaltered (point A). On the other hand, the streamwise coordinate, where the maximum value occurs, decreases with increasing frequency, as shown in the comparison of point B position in Figs. 3, 4, 5 and 6. As a consequence, the entire evolution (blowing and suction phases) of the peaks envelope shortens with the increasing frequencies; the last peak (corresponding to $\Phi = 360°$) occurs a $x/r_x = 7.2$ for $St = 0.23$ and is anticipated to $x/r_x = 6$ for $St = 0.31$ (Point C). The trend is also confirmed for the highest frequency ($x/r_x = 4.8$). On the other hand, the second peak, i.e. the one in the origin proximity, seems not to be affected by the frequency, and remains approximatively constant for each case. Further analysis is necessary by comparing the time-averaged total entrainment along with the reference line at different Strouhal numbers: results are reported in Figure 7. The average velocity during a pulsation period increases as a function of frequency. In particular, the velocity along the reference line increases in a streamwise zone between $x/r_x = 2$ and $x/r_x = 6$ slightly decreases for $x/r_x > 6$ (Fig. 7a). The overall effect is positive, as measured with the integral of the area below the curves (Fig. 7b). Thus, the entrainment effects are boosted up with the Strouhal number increase.

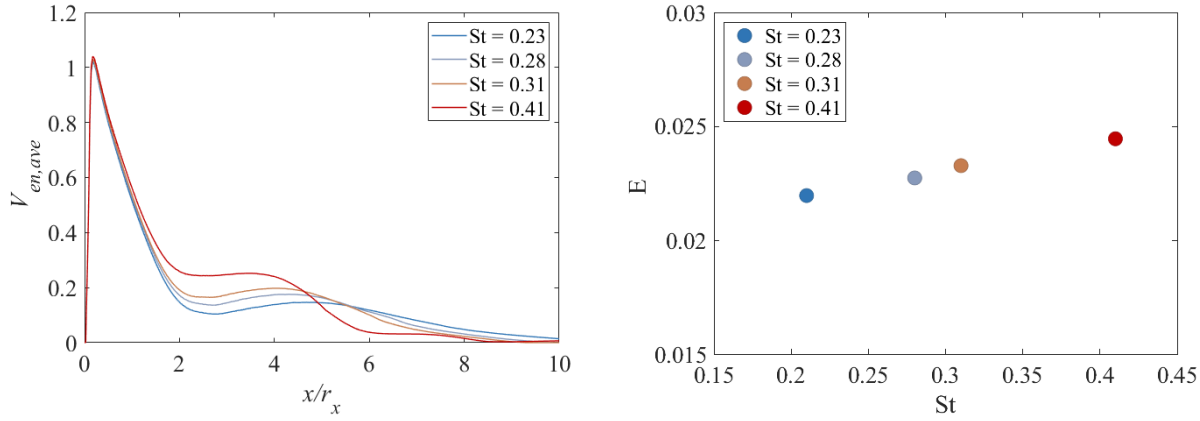

(a) Time Averaged Entrainment: $\phi = 0 \div 360°$

(b) Total Entrainment

Fig. 7 Comparison among Velocity Averages and total Entrainment along the reference line at different Strouhal numbers.

V. Comparison between Steady and Unsteady Analyses

Following the unsteady analysis, this section aims at determining a correlation between the unsteady jet at a given frequency and an equivalent steady-state jet exhaust velocity that could match the unsteady flow entrainment rate evaluated along at a specific reference line. To this purpose, the quantities needed to be considered for the comparison have to be carefully selected: the steady-state jet does not include a suction phase; therefore, only the blowing phase of the unsteady jet is accounted for the comparison. To this purpose, an equivalent metric for the entrainment ratio is defined by taking the integral over the $[0 : \pi]$ phase-averaged entrainment velocity, $\bar{V}_{en}$. Thus, we compute the phase average of the entrainment speed to the first half of the pulsating period, corresponding to the blowing phase. The following equation holds:

$$E = \int_{x_0}^{x_F} \bar{V}_{en} dx \tag{4}$$

being x_0 and x_F the initial and the final interval locations over the selected entrainment line.

Five samples are considered in ejected mass flow to assess the correlation between the jet's velocity and the entrainment. Steady-state analyses are performed for each sample, and the respective entrainment ratio values at the chosen reference line are evaluated. The results of the computations are reported in Table 2. As the reader can notice, in steady-state cases, the entrainment ratio is a weak decreasing function of the ejected non-dimensional specific mass flow (hence, jet velocity). Here $\dot{m}$ is the specific mass flow while $\dot{m}^\star$ denotes the reference mass flow and it is equal to 80 $kgm^{-2}s^{-1}$.

Sample	$\dot{m}/\dot{m}^\star$	V_j/V_∞	E
1	1.000	2.33	0.106551
2	1.125	2.59	0.104775
3	1.250	2.84	0.103137
4	1.375	3.07	0.101626
5	1.500	3.30	0.100213

Table 2 Results of the steady-state jet analysis.

The findings are used to establish a correlation between the actuator mass flow and the entrainment level. The correlation is linear. Therefore, a regression line is determined over the sampled points. The regression allows estimating the mass-flux necessary to obtain the same entrainment of the unsteady jets. Thus, CFD evaluations on the estimated mass flow are carried out to verify the prediction accuracy, and the results are listed in Table 3, demonstrating a fair

prediction capability of the regression model.

Figure 8 shows the comparison in terms of entrainment curves for the $St = 0.41$ case: although the steady-state entrainment is very close to the unsteady target entrainment, the two curves have different shapes. Two main differences between the curves can be appreciated: (a) the left-side peak of the steady-state curve is minimal compared to one of the unsteady curves. This is justified by the fact that the unsteady jet behaves as additional outer-to-jet fluid entrainment from the mushroom-head of the starting jet (which can be seen in Figure 2); (b) in the central and right-side of the chart, the unsteady curve has a more significant oscillation than the steady line. This is because the unsteady curves also show the influence of the previous jets. A chart that correlates the steady-state jet velocity to the correspondent unsteady

Ref. Strouhal	Est. V_j/V_∞	CFD V_j/V_∞	Δ%
0.23	2.17	2.14	-1.38%
0.28	2.57	2.58	+0.38%
0.31	2.67	2.68	+0.37%
0.41	2.35	2.33	-0.85%

Table 3 Steady-state jet analysis: verifications.

jet frequency is presented in Figure 9. As apparent, the distribution of equivalent steady jet velocity as a function of frequency suggests the occurrence of a maximum, which is positioned between the highest two frequencies analysed.

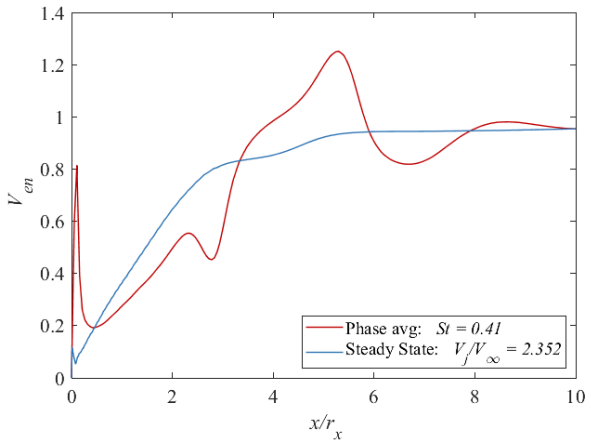

Fig. 8 Comparison between the steady-state jet V_{en} curve and the correspondent curve at St = 0.41.

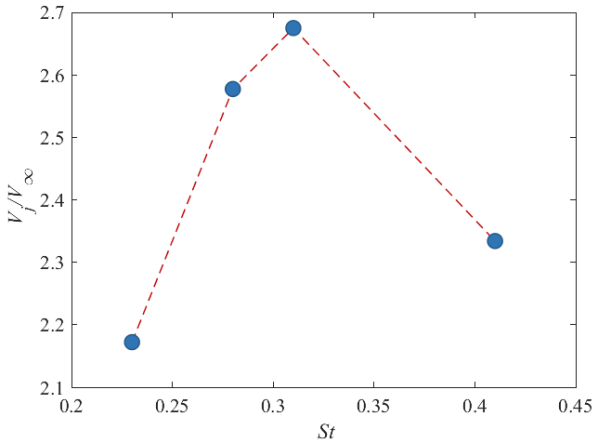

Fig. 9 Correlation between the steady-state jet velocity and the unsteady jet Strouhal Number.

VI. Conclusions

The present work provides a suitable steady-state reduced model with equivalent entrainment level of a realistic unsteady jet. Based on the steady analyses, the entrainment effects provided by the synthetic pulsed jets play a crucial role in the flow mixing. To efficiently carry out the analyses, the simplified domain from the CFDVAL Workshop [11] is used rather than the whole wing/nacelle installation. Consequently, the computational time and resources are highly reduced compared to the entire geometry while the flow physics is well captured.

In particular, a simple cross-flow without simulation of the whole actuator geometry is chosen for determining the influence of pulsed jet frequency on the entrainment. In addition, a proper metric for entrainment evaluation is defined based on the most recent published literature [8]. Several unsteady simulations are performed for a range of Strouhal numbers to illustrate the effects of varying the frequency of the pulsed jet. The results in terms of entrainment rate are presented and discussed. Finally, a series of steady analyses are performed to match the unsteady results, determining a corresponding velocity for jets to match the entrainment. In conclusion, the distribution of equivalent steady jet velocity as a function of frequency suggests a maximum occurrence.

Future investigations should consider a broader range of frequencies to compute such conditions accurately and derive a more general law.

Acknowledgements

This study is financed by the Clean Sky 2 project X-Pulse (High Fidelity time-accurate CFD Simulations). The project has received funding from the European Union's Horizon 2020 research and innovation programme under grant agreement number 738172.
The authors also acknowledge the CINECA award under the ISCRA initiative, for the availability of high performance computing resources and support.

References

[1] Han, D., and Mungal, M. G., "Direct measurement of entrainment in reacting/nonreacting turbulent jets," *Combustion and Flame*, 2001. https://doi.org/10.1016/S0010-2180(00)00211-X.

[2] Dabiri, J. O., and Gharib, M., "Fluid entrainment by isolated vortex rings," *Journal of Fluid Mechanics*, 2004. https://doi.org/10.1017/S0022112004009784.

[3] Olcay, A. B., and Krueger, P. S., "Measurement of ambient fluid entrainment during laminar vortex ring formation," *Experiments in Fluids*, 2008. https://doi.org/10.1007/s00348-007-0397-9.

[4] Raju, R., Aram, E., Mittal, R., and Cattafesta, L., "Simple models of zero-net mass-flux," *International journal of Flow Control*, 2009.

[5] El Hassan, M., and Meslem, A., "Time-resolved stereoscopic particle image velocimetry investigation of the entrainment in the near field of circular daisy-shaped orifice jets," *Physics of Fluids*, 2010. https://doi.org/10.1063/1.3358465.

[6] Sau, R., and Mahesh, K., "Optimization of pulsed jets in crossflow," *Journal of Fluid Mechanics*, 2010. https://doi.org/10.1017/S0022112010000388.

[7] Möller, G., Detert, M., and Boes, R. M., "Vortex-induced air entrainment rates at intakes," *Journal of Hydraulic Engineering*, 2015. https://doi.org/10.1061/(ASCE)HY.1943-7900.0001036.

[8] Berk, T., Medjnoun, T., and Ganapathisubramani, B., "Entrainment effects in periodic forcing of the flow over a backward-facing step," *Physical Review Fluids*, 2017. https://doi.org/10.1103/PhysRevFluids.2.074605.

[9] Stella, F., Mazellier, N., Joseph, P., and Kourta, A., "Mass entrainment-based model for separating flows," *Physical Review Fluids*, 2018. https://doi.org/10.1103/PhysRevFluids.3.114702.

[10] "X-Pulse - High Fidelity time-accurate CFD Simulations," *Clean Sky 2 Joint Undertaking*, 2020.

[11] "NASA 2004 CFD Validation Workshop," *https://turbmodels.larc.nasa.gov/Other*$_{e}$*xp*$_{D}$*ata/cfdval2004*$_{e}$*xp.html*, 2004.